


RESEARCH ARTICLE

Open Access



Daytime F-region irregularity triggered by rocket-induced ionospheric hole over low latitude

Guozhu Li^{1,2*} , Baiqi Ning^{1,2}, M. A. Abdu^{3,4}, Chi Wang², Yuichi Otsuka⁵, Weixing Wan¹, Jiuhou Lei⁶, Michi Nishioka⁷, Takuya Tsugawa⁷, Lianhuan Hu^{1,8}, Guotao Yang² and Chunxiao Yan^{2,9}

Abstract

Unexpected daytime F-region irregularities following the appearance of an ionospheric hole have been observed over low latitude. The irregularities developed initially above the F-region peak height (~ 360 km) with a thickness of about 30 km and an east-west extension of more than 200 km around 1057 LT and then expanded upward to 500 km altitude behaving like the equatorial spread-F (ESF) irregularities of the nighttime ionosphere. These daytime F-region irregularities cannot be explained on basis of an earlier suggestion that the F-region irregularities observed during daytime are the continuation of the irregularities initially generated on the previous night. Based on the coincidence, both in space and time, with the appearance of an ionospheric hole, which was generated after the passage of a rocket, we conclude that the daytime F-region irregularities must have been artificially generated locally through a manifestation of plasma instability triggered by the rocket exhaust-induced ionospheric hole over low latitude.

Keywords: Daytime F-region irregularity, Ionospheric hole, Rocket exhaust

Introduction

Equatorial spread-F (ESF), which contains plasma irregularities of wide-ranging scale sizes, commonly occurs in the nighttime equatorial ionospheric F-region with a maximum occurrence during pre-midnight hours (Kelley 2009 and the references therein). For many years there have been only a few cases of F-region irregularities observed over equatorial and low latitudes during daytime (e.g., Fukao et al. 2003; Shume et al. 2013 and references therein). The daytime F-region irregularities can be categorized into two types. One type is due to the long lifetime of ESF irregularities initially generated on the previous night or near sunrise through the Rayleigh-Taylor instability during active geomagnetic conditions (Fukao et al. 2003; Li et al. 2010; Huang et al. 2013). By using total electron content (TEC) observations from a globally distributed GPS receiver network, together with ionosonde data and satellite

in situ plasma density observations made during the geomagnetic storms of July 2004, Li et al. (2010) found that ESF irregularities were generated sequentially after sunset over a large longitude region of about 180° (from American to Southeast Asian longitudes) and continued until late morning (~ 0900 LT). More recently, Huang et al. (2013) reported C/NOFS satellite in situ observations of long-lasting ESF irregularities, which initially occurred at post-midnight and survived until noontime with a lifetime of 12 h. Most of the daytime F-region irregularities reported in the literatures belong to this type and have been suggested to be triggered by electric field and/or wind disturbances associated with geomagnetic activity (e.g., Abdu 2012).

Another type of daytime F-region irregularities was first observed by the Jicamarca radar (Woodman et al. 1985; Chau and Woodman 2001) and then by the Sao Luis and Fuke VHF radars (Shume et al. 2013; Chen et al. 2017) during quiet geomagnetic conditions. These irregularities, which seem unlikely to cause any diffuse echo in ionosonde ionogram, were very rarely observed and called as ESF-like irregularities (Chau and Woodman 2001). Radar observations showed that the backscatter echoes from these irregularities usually persist for a short

* Correspondence: gzlee@mail.jiggcas.ac.cn

¹Key Laboratory of Earth and Planetary Physics, Institute of Geology and Geophysics, Chinese Academy of Sciences, Beijing, China

²State Key Laboratory of Space Weather, National Space Science Center, Chinese Academy of Sciences, Beijing, China

Full list of author information is available at the end of the article

time of 1–2 h in radar range-time-intensity (RTI) maps and have extremely narrow Doppler spectral width and nearly zero Doppler velocity, except the case by Shume et al. (2013) where a large upward Doppler velocity of more than 100 m/s was detected. Due to the rarity of daytime F-region irregularities, and the difficulty in determining when and where these irregularities are initially generated, their generation mechanism still remains unresolved.

In this paper, we report observations of artificially generated daytime F-region irregularities on May 30, 2016 (the minimum Dst – 16 nT), by the Fuke VHF coherent scatter radar (19.3° N, 109.1° E; dip latitude 14° N). This radar, with a multi-beam steering capability, is able to distinguish the F-region irregularities generated locally from those drifted from elsewhere. Unlike the daytime F-region irregularities reported previously that were often suggested to be the continuation of naturally occurring nighttime irregularities (e.g., Li et al. 2010; Huang et al. 2013; Chen et al. 2017), the present F-region irregularities, with Doppler spectra similar to that of the ESF-like irregularities (e.g., Chau and Woodman 2001), are demonstrated to be initially generated during daytime. Most interestingly, about 12 min before the generation of F-region irregularities, an ionospheric hole identified by TEC reductions with magnitudes of up to ~23% was detected by a global navigation satellite system (GNSS) receiver network over low latitude. The track of the ionospheric hole was found to be in good coincidence with the track left by passage of a rocket both in space and time. We discuss possible mechanisms responsible for the present daytime F-region irregularities, which evolved from the rocket exhaust-induced ionospheric hole.

Methods/Experimental

The Fuke VHF radar, with a peak power of 54 kW and an operational frequency of 47 MHz, was installed in 2010 under the support of the Chinese Meridian Project to study the low-latitude ionospheric irregularities (Wang 2010). On the day (May 30, 2016) when the F-region irregularities were observed, the radar was operated with a 7-beam steering mode that formed a field of view of 45° (in east-west direction) to observe E- and F-region plasma irregularities. The major operational parameters were set as follows: a pulse repetition frequency of 200 Hz, 13-bit Barker coded pulse, coherent integration number 2, and a range resolution of 0.711 km. The seven beams were directed at the azimuth angles of 22.5°, 15°, 7.5°, 0°, –7.5°, –15°, and –22.5°, respectively (at a zenith angle of 28°). Considering the wide 3 dB beam width of the radar (21° in north-south direction), the perpendicularity between the radar line of sight and the geomagnetic field line can be met for all the seven beams to detect both ionospheric E- and F-region irregularities (e.g., Li et al. 2017). The Doppler velocity and spectral width were

calculated offline from the complex raw signal returns of the radar by employing a 256-point FFT algorithm and the moment method (e.g., Ning et al. 2012), with velocity window of ± 160 m/s and velocity resolution of ~ 1.25 m/s.

Results

Figure 1a shows the Fuke radar (beam 6) observations on May 30, 2016, when the daytime F-region irregularities were detected. As a comparison, a typical case of nighttime ESF irregularities observed by the radar (beam 6) on October 26, 2015, is shown in Fig. 1b. The F-region peak heights (hmF2) obtained from the Sanya ionosonde (situated at a distance of about 120 km from Fuke) are superposed in the two RTI plots. As shown in Fig. 1a, the daytime F-region irregularities, which got initiated at 1057 LT, were seen as a backscattering layer around 360 km altitude, which then gradually rose to higher altitudes. There are two possibilities that could produce an ascending structure of backscatter echoes in the radar RTI map. One is linked with an irregularity layer elevated to higher altitude in the radar field of view, and another is that an irregularity layer situated at constant altitudes but tilted in longitude and drifts across the radar field of view. For the present case, the Fuke radar multi-beam measurements rule out the latter possibility because no tilted structure was detected in the fan sector maps (which will be shown in Fig. 2).

It is seen from Fig. 1a that in about 36 min, the irregularity layer rapidly evolved into a nearly vertical irregularity structure extending up to 500 km altitude into the topside ionosphere. Such a vertical structure of the daytime F-region irregularities appears similar to that of the nighttime ESF irregularities shown in panel b. The nighttime (post-sunset) ESF structure started from F-region bottomside where positive (upward) plasma density gradients favoring for plasma instability development usually exist and grew up to 450 km into the topside. However, for the present case, the starting altitude of the daytime irregularity structure is near/above the F-region peak (~360 km) where the background plasma density gradient is usually not favorable for plasma instability. The cause why the daytime F-region irregularities started from F-region peak will be discussed in the later section. Figure 1c–f show the Doppler velocities and spectral widths as functions of range and time. An example of Doppler spectra of the daytime irregularities measured at 1133 LT (0415 UT) on May 30, 2016, at three different height regions, is inset in the left middle panels. The spectra from the height region of 517–523 km clearly show that these irregularities have very small Doppler velocities and extremely narrow spectral widths, which, in general, ranged between ± 4 and 2–6 m/s, respectively, and are obviously different from those of the nighttime ESF irregularities (not shown here). These

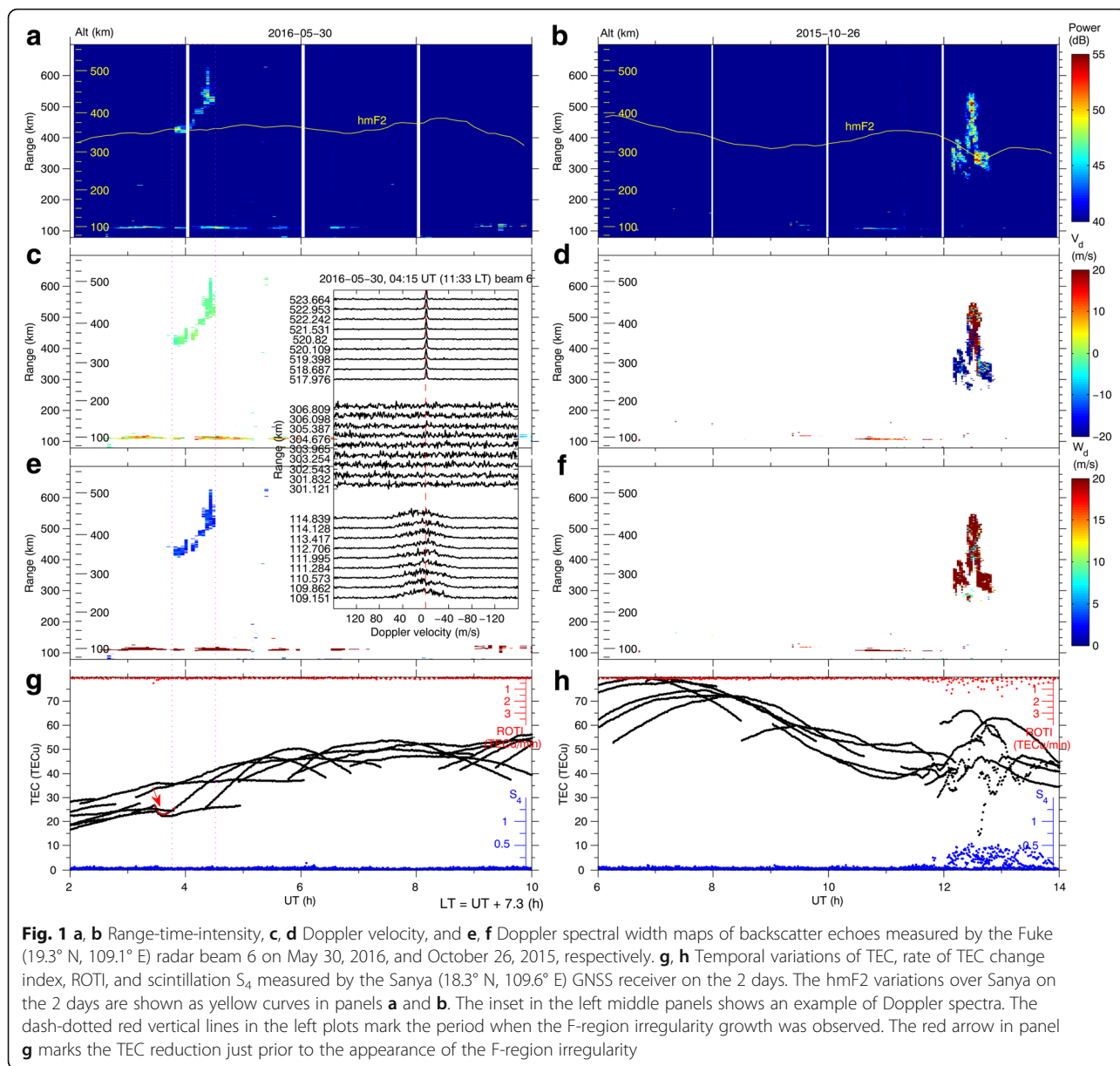


Fig. 1 a, b Range-time-intensity, c, d Doppler velocity, and e, f Doppler spectral width maps of backscatter echoes measured by the Fuke (19.3° N, 109.1° E) radar beam 6 on May 30, 2016, and October 26, 2015, respectively. g, h Temporal variations of TEC, rate of TEC change index, ROTI, and scintillation S_4 measured by the Sanya (18.3° N, 109.6° E) GNSS receiver on the 2 days. The hmF2 variations over Sanya on the 2 days are shown as yellow curves in panels a and b. The inset in the left middle panels shows an example of Doppler spectra. The dash-dotted red vertical lines in the left plots mark the period when the F-region irregularity growth was observed. The red arrow in panel g marks the TEC reduction just prior to the appearance of the F-region irregularity

spectral characteristics suggest that these daytime F-region irregularities resemble the so-called daytime ESF-like irregularities with high magnetic aspect sensitivity discussed by Chau and Woodman (2001).

In Fig. 1g, h, we show the variations of vertical TEC, rate of TEC change index, ROTI (Pi et al. 1997), and amplitude scintillation index S_4 (for all PRNs with elevation angle $> 30^\circ$) measured by a Novatel GNSS TEC/scintillation receiver over Sanya on May 30, 2016, and Oct. 26, 2015, respectively. We may note that the nighttime/post-sunset ESF irregularities produced ionospheric scintillations (maximum S_4 up to 0.5) and fast TEC fluctuations (maximum ROTI up to ~ 1.5 TECu/min) (Fig. 1h), as to be expected, whereas no scintillation, fast

TEC fluctuation, and diffuse echo trace in ionogram (figure not shown here) was detected during the presence of the daytime F-region irregularities (Fig. 1g). Of particular interest is that just before the appearance of the daytime F-region irregularities in the radar beams, a TEC reduction (as a negative kink in TEC marked by an arrow in Fig. 1g) was observed along one satellite-receiver link around 1045 LT (0327 UT). The nature of TEC reduction, which has a relatively slow recovery process, is different from the fast TEC fluctuations (appearing along a few satellite-receiver links) caused by ESF irregularities (Fig. 1h). Later in the paper, we will show the measurements by a GNSS TEC receiver network situated around Southern China, which explicitly link the TEC reduction to a background ionospheric

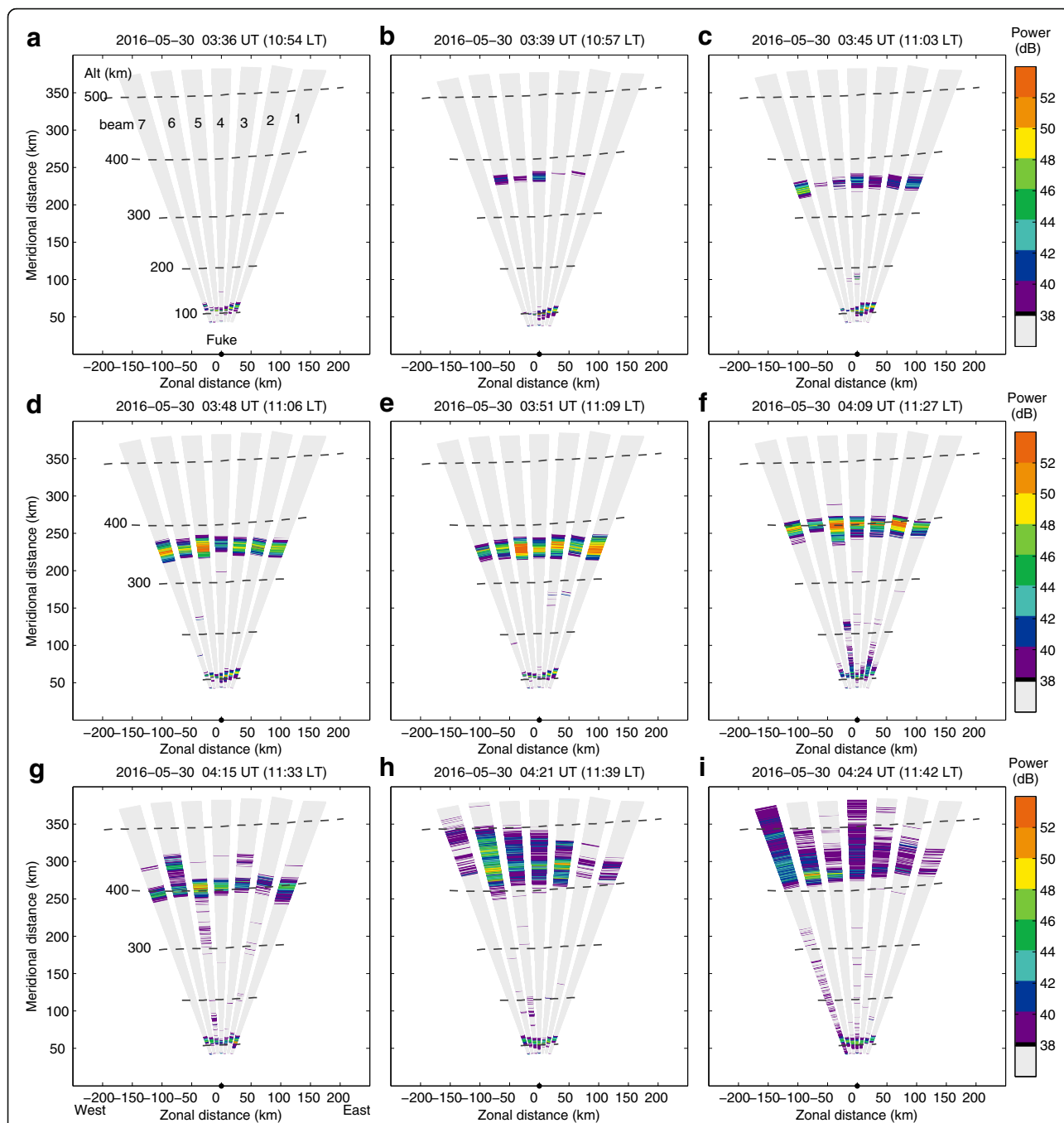


Fig. 2 a-i The fan sector maps of echo power (in dB) taken from 1054 LT (0336 UT) to 1142 LT (0424 UT) showing the onset and growth of F-region irregularities. The horizontal and vertical axes in each plot represent the zonal and meridional distance from the radar site on the Earth’s surface, respectively. The horizontal dashed lines in each plot show the altitudes (from 100 to 500 km with an altitude interval of 100 km) where the radar line of sight is perpendicular to the geomagnetic field. The zonal width of each beam indicates the half power beam width

hole generated by the passage of a rocket (~ 300 km away from Sanya in longitude) on May 30, 2016.

To examine the spatial distribution of the daytime F-region irregularities and its temporal variation, we show in Fig. 2 a series of fan sector maps of echo power (in dB) from all the seven beams of the Fuke radar, as a function

of distances in the east-west and north-south directions. The superposed dashed lines in each plot show the given altitudes (from 100 to 500 km with an altitude interval of 100 km) where the radar line of sight is perpendicular to the geomagnetic field. The top three maps, taken from 1054 LT (0336 UT) to 1103 LT (0345 UT), show the initial

generation of irregularity layer around the F-region peak height of ~ 360 km. When the irregularities were first detected in the 1057 LT (0339 UT) map, they were confined to the beams 2 to 6 only. In the map taken 6 min later (at 11:03 LT), the irregularity generation had already extended in east-west direction occupying all the radar beams and perhaps well beyond. The structure was confined to a small range of altitude but occupied an extended range of longitude, that is, more than 200 km in the east-west direction. Due to the limited field of view, the radar could not cover the exact longitudinal extent of the thin irregularity layer. It is evident from Fig. 2d–f that the irregularity layer rose from 360 to 400 km altitude with a mean velocity of about 30 m/s. The background plasma vertical drift was found ranging between 10 and 20 m/s around 1100 LT over Southeast Asia (see Figure 9 of Patra et al. 2012). During the rising process, the irregularities seemed not to extend in altitude with time, being confined to a layer with thickness of about 30 km. After the layer rose to about 400 km altitude (Fig. 2g–i), the irregularities in a zonal dimension of about 150 km, mostly in the western beams, expanded abruptly up to high altitude, 500 km or greater. The degree of irregularity upward growth appears to be less pronounced in the eastern beams than it is in the western beams (as is evident in Fig. 2h, i), which seems to be due to the fact, as illustrated in Fig. 3, that eastern beams are pointed to a region closer to the TEC depletion eastern boundary, whereas the western beams cover more of the central regions of the depletion where the depletion depth could be larger. The irregularities decayed and disappeared around 1151 LT (0433 UT).

Discussion

For the present case, the Fuke radar multi-beam steering measurements clearly reveal that the daytime F-region irregularities were not the continuation of nighttime ESF irregularities but generated locally over the longitudes scanned by the radar during 1057–1151 LT (0339–0433 UT). Before we discuss possible mechanisms responsible for the daytime F-region irregularities, it may be relevant to mention the two possibilities for the generation of nighttime F-region irregularities over low latitude: (1) The ESF plasma bubble generation after sunset in equatorial F-region through the generalized Rayleigh-Taylor instability and their magnetic field line mapping to low latitudes in both hemispheres where meter scale irregularities develop locally through the non-linear cascade process (see also Otsuka et al. 2002; Patra and Phanikumar 2009). This is the case for the F-region irregularities observed after sunset during equinoctial months (ESF high occurrence season) over Southeast Asia low latitude (for example Fuke and Sanya) (e.g., Li et al. 2012, 2016); and (2) Meter scale irregularities generated locally over low latitude not being associated with large scale plasma

bubbles. The F-region irregularities observed at midnight/post-midnight during summer months over low/middle latitudes in East/Southeast Asia have been suggested to be generated locally by the medium-scale traveling ionospheric disturbance (MSTID) and driven by gradient-drift instability mechanism (e.g., Yokoyama et al. 2011 and the references therein).

For the present F-region irregularities that developed during daytime, the key question lies in the fact that the normally present perturbation factors under the daytime F-region conditions are expected to be too weak to favor any instability development over equatorial and low latitudes (e.g., Kelley and Ilma 2016). As regards the initiation and growth of the Rayleigh-Taylor instability over magnetic equator and of the MSTID-driven gradient drift instability over low latitude, an important requirement is plasma density perturbation with its associated polarization electric field being present at the ionospheric F-region. However, during daytime, the E-region conductivity is obviously larger than that of nighttime that can lead to a reduction of the F-region polarization electric fields (Kelley 2009). Under such condition, the factors, for example the plasma density gradient and/or its associated polarization electric field required to initiate instability growth during daytime, operating against the inherently stable conditions of the daytime ionosphere, should have abnormally larger amplitude than that required for instability growth in the nighttime ionosphere.

In this context we may note from Fig. 1g that an obvious TEC reduction was observed just prior to the detection of the daytime F-region irregularities. To obtain the spatial coverage of TEC reduction, we investigated the TEC data obtained from GNSS receivers and Beidou geostationary satellite receivers situated around Southern China. Figure 3a shows the geographic locations of ionospheric pierce points (IPP, shown as curves and dots) for the GNSS satellite-receiver links (with elevation angle $> 30^\circ$) measured during the period 0315–0345 UT (1033–1103 LT), May 30, 2016. Note that the dots represent the fixed IPPs for the Beidou geostationary satellite-receiver links. From this plot we can see that TEC reductions (marked by blue) were detected at latitudes higher than $\sim 12\text{--}13^\circ$ N, around the longitudes where the daytime F-region irregularities were observed. Figure 3b shows the temporal variation of TEC reductions measured at the fixed IPPs from higher to lower latitudes (marked by blue dots in Fig. 3a). Two notable features can be seen from this plot: (1) the TEC reductions initially appeared around 1045 LT (0327 UT, marked by a blue dotted vertical line) in a wide latitude region, about 12 min before the generation of daytime F-region irregularity; and (2) the time when the TEC maximum reductions were observed (marked by a red

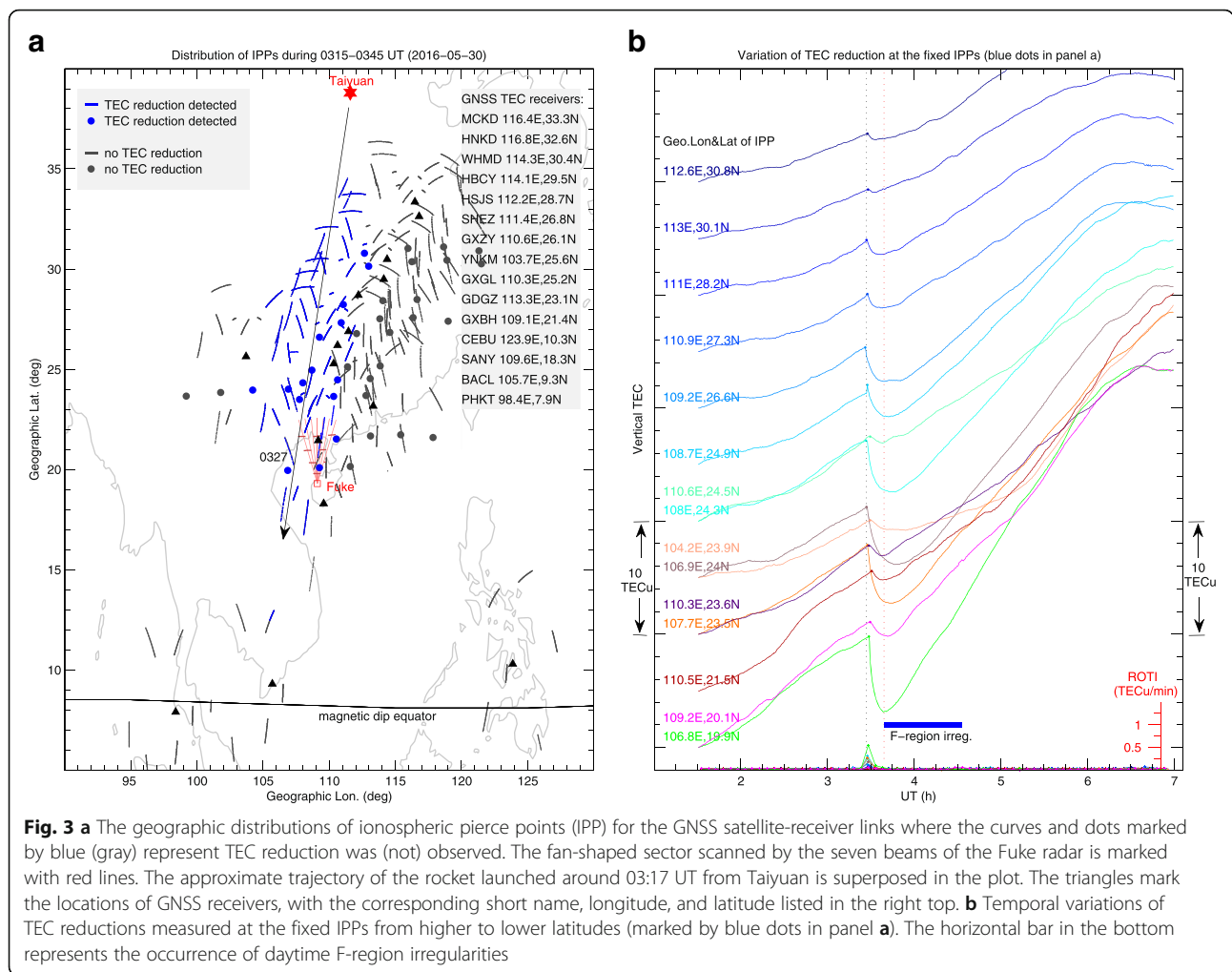


Fig. 3 a The geographic distributions of ionospheric pierce points (IPP) for the GNSS satellite-receiver links where the curves and dots marked by blue (gray) represent TEC reduction was (not) observed. The fan-shaped sector scanned by the seven beams of the Fuke radar is marked with red lines. The approximate trajectory of the rocket launched around 03:17 UT from Taiyuan is superposed in the plot. The triangles mark the locations of GNSS receivers, with the corresponding short name, longitude, and latitude listed in the right top. **b** Temporal variations of TEC reductions measured at the fixed IPPs from higher to lower latitudes (marked by blue dots in panel a). The horizontal bar in the bottom represents the occurrence of daytime F-region irregularities

dotted vertical line) corresponds to the initial generation of daytime F-region irregularity (with the duration indicated by a blue horizontal bar). During the presence of daytime F-region irregularities (3-meter scale), no amplitude scintillations (small S_4) and obvious fast fluctuations of TEC (small ROTI) were detected around the region where the 3-meter scale irregularities were observed. Due to the significant recovery of background plasma density (increased by ~ 10 TECu in 1 h), the absolute perturbation density induced by the irregularities could be very low and hard to be detected in TEC.

As regards the generation of TEC reductions, we note from the CCTV news (tv.cctv.com) that China launched a sun-synchronous satellite using a Long March-4B rocket from Taiyuan on May 30, 2016. The arrow superposed in Fig. 3a represents the approximate trajectory of the rocket projected onto the Earth's surface (from news press). The rocket passed over southern China (near the location where the daytime F-region irregularities were observed) around 1045 LT (0327 UT), being well coincident with the detection of TEC reductions both in space

and time. Further details on the rocket trajectory and exhaust information are beyond the scope of this study and will not be addressed here. It is well known from earlier studies that the rocket exhaust, which consists of CO_2 , H_2O , and N_2 , could cause quick reduction in the background ionospheric F-region primary ion (O^+) density through chemical reactions and produce an ionospheric hole (e.g., Bernhardt et al. 2001; Mendillo et al. 2008; Nakashima and Heki 2014). The coincident observations of the TEC reductions and the rocket passage, both in time and space, reveal that the TEC reductions must be associated with a background ionospheric hole produced by the rocket exhaust. The hole should be centered around the rocket release altitude (e.g., Bernhardt et al. 1998). For the present case, the rocket altitude (near the location where the daytime F-region irregularities were observed) is approximately 350 km, right near the F-region peak height.

Based on the sequential observations of ionospheric hole, followed by the appearance of thin irregularity layer evolving into plume-like irregularities expanding to

high altitude, which occurred promptly after the passage of the rocket over Southern China, we may conclude that the daytime F-region irregularities in the present study must have been artificially triggered by the rocket exhaust-induced ionospheric hole around the F-region peak (~ 350 km). Although earlier rocket release experiments have shown the occurrences of artificially generated F-region irregularities (e.g., Bernhardt et al. 2012), the present F-region irregularities were observed at daytime with a form similar to that of naturally generated ESF in radar RTI map. Based on the observations of TEC reductions shown in Fig. 3b, the fractional decrease in the local electron density, constituting the present ionospheric hole, could provide plasma density gradients significantly larger than that required for nighttime F-region irregularity development. In Fig. 3b, we note that the maximum TEC reduction is about 7 TECu that represents a perturbation by 23%, of the total unperturbed TEC value, which is ~ 30 TECu. This value is significantly larger than the perturbation (of about 2–5%) nominally required for F-region irregularity development under typical post-sunset/nighttime conditions (e.g., Zalesak et al. 1982; Yokoyama et al. 2011). The deep ionospheric hole representing significant depletion in the background plasma density that is obtained here in fact describes a plasma density depletion structure necessarily with large upward density gradient around the F-region peak. By using the simultaneous observations of 3-meter scale irregularities and of plasma density depletions with the low latitude Kototabang VHF radar and all-sky airglow imager, respectively, Otsuka et al. (2004) reported that the most intense backscatter (induced by 3-meter scale irregularities) came from the deepest plasma density depletion region. They suggested that the 3-meter scale irregularities were generated through the lower-hybrid-drift instability. For the present study, the lower-hybrid-drift instability could also operate in the deepest depletion region with large density gradients and produce the 3-meter scale irregularities.

According to the empirical F-region plasma drift model (Fejer et al. 2008), the plasma drifts upward during daytime under the background eastward electric field. Through investigating the daytime 150 km echoes from Gadanki and Kototabang VHF radars, Patra et al. (2012) reported that the upward drifts over Kototabang (10° away from Fuke in longitude) range between 10 and 20 m/s at 1100 LT. For the present case, the uplift of the irregularity layer with a velocity of about 30 m/s, shown in Fig. 2d–f, is larger than the upward drifts of background plasma shown in Patra et al. (2012). Under the force of gravity and the Pedersen current due the background eastward electric field, a relatively more intense polarization zonal (eastward) electric field could be set up in the deep ionospheric hole characterized by a

significant TEC perturbation, 23% of the total unperturbed TEC. Earlier Millstone Hill ISR measurements have provided direct observational evidences on the sustenance of daytime F-region polarization electric field (Buonsanto 1994). For the present case, if the polarization electric field generated in the deep ionospheric hole was not well shorted out by the E-region conductivity, it would enhance the upward drift. It has been shown that the sustainability of F-region polarization electric field would depend upon the ratio of the field line-integrated conductivity of the F-region to that of the sum of F- and E-regions (that is, $\Sigma_F^P / \Sigma_{E+F}^P$) (Kelley 2009). Whereas the E-region conductivity at daytime is obviously larger than that of nighttime, detailed calculation by Abdu et al. (2015) based on a low-to-mid latitude ionospheric model simulated by the SUPIM (Sheffield University Plasmasphere Ionosphere Model, Bailey et al. 1997) has shown that the value of the ratio $\Sigma_F^P / \Sigma_{E+F}^P$ can be of the order of 0.8–0.9 under near-midday conditions, thereby assuring the prevalence of a major portion of the F-region polarization electric field. We surmise that the extremely large density gradient as characterized by the ionospheric hole, together with the potentially survived eastward polarization electric field, could be intense enough to upset the stability of the normal daytime ionosphere, thereby leading to the accelerated growth of F-region irregularities that promptly followed, as observed by the Fuke radar. Further efforts will be made to better understand this type of phenomenon in the future.

Conclusions

This study has presented an unexpected case of F-region irregularities that were artificially generated in the daytime ionosphere over low latitude. The most interesting characteristics of these irregularities are their initial generation as a thin layer and evolution marked by slow rise to higher altitude, followed by rapid evolution into a vertical structure, resembling closely those of nighttime ESF irregularities. However, it is difficult to explain their generation through instability drivers of intensity similar to those of the natural sources that drive the instability responsible for the quiet nighttime F-region irregularities, that is, the naturally occurring ESF irregularities. The simultaneous TEC measurements from a GNSS- and geostationary-satellite receiver network around Southern China detected depletions in TEC promptly after the passage of a rocket. The degree of the TEC depletion indicated the presence of a deep plasma hole created by the rocket exhaust in the background F-region. The plasma hole resulted in the prompt generation (within a few minutes) of the daytime F-region irregularity structure detected by the simultaneously operated Fuke radar. A possible explanation of this artificially generated

daytime F-region irregularity structure is offered based on (1) the sufficiently intense density gradient that characterizes the plasma hole, (2) such gradient leading to the development of polarization electric field (induced by the background zonal electric field) which potentially survived at daytime, and (3) the factors (1) and (2) driving plasma instability to be followed by Rayleigh-Taylor mechanism responsible for the rising plume like structure. As regards the generation of 3-meter scale irregularities inside the structure, the lower-hybrid-drift instability excited by large density gradients in the deepest depletion region could be a possible mechanism. The present observations of daytime F-region irregularities triggered by the rocket exhaust-induced ionospheric hole may add further evidence on the possibility of artificial triggering of ESF irregularities.

Abbreviations

C/NOFS: Communications/Navigation Outage Forecasting System; ESF: Equatorial spread-F; GNSS: Global navigation satellite system; MSTID: Medium-scale traveling ionospheric disturbance; ROTI: Rate of TEC change index; RTI: Range-time-intensity; TEC: Total electron content

Acknowledgements

The data used in this research are supported in part by the Chinese Meridian Project and the Data Center for Geophysics, National Earth System Science Data Sharing Infrastructure (<http://wdc.geophys.cn/>). MAA acknowledges the support from CAPES for a senior visiting professorship at ITA.

Funding

This study was carried out as a part of the project funded by the National Natural Science Foundation of China (41422404 and 41727803).

Availability of data and materials

All the data used in this study are available from the corresponding author on request.

Authors' contributions

GL conducted part of the Fuke radar and TEC data analysis and wrote the paper with significant contributions from MAA. BN and CW are the principal investigators of the TEC monitoring network and the Fuke VHF radar in China, respectively. WW and JL are the co-investigators of the TEC network. YO, MN, and TT provided the data of CEBU, BAOL, and PHKT from SEALION and assisted the data analysis. LH conducted part of the TEC data analysis. GY and CY conducted part of the radar data analysis. All authors contributed and approved the final version of the paper.

Competing interests

The authors declare that they have no competing interests.

Publisher's Note

Springer Nature remains neutral with regard to jurisdictional claims in published maps and institutional affiliations.

Author details

¹Key Laboratory of Earth and Planetary Physics, Institute of Geology and Geophysics, Chinese Academy of Sciences, Beijing, China. ²State Key Laboratory of Space Weather, National Space Science Center, Chinese Academy of Sciences, Beijing, China. ³Instituto Nacional de Pesquisas Espaciais (INPE), Sao Jose dos Campos, SP, Brazil. ⁴Instituto Tecnológico de Aeronautica (ITA), Sao Jose dos Campos, SP, Brazil. ⁵Institute for Space-Earth Environmental Research, Nagoya University, Nagoya, Japan. ⁶School of Earth and Space Science, University of Science and Technology of China, Hefei, China. ⁷National Institute of Information and Communications Technology, Tokyo, Japan. ⁸Beijing National Observatory of Space Environment, Institute of Geology and Geophysics, Chinese Academy of Sciences, Beijing, China.

⁹Hainan National Observatory of Space Weather, National Space Science Center, Chinese Academy of Sciences, Beijing, China.

Received: 28 June 2017 Accepted: 12 February 2018

Published online: 20 February 2018

References

- Abdu MA (2012) Equatorial spread F/plasma bubble irregularities under storm time disturbance electric fields. *J Atmos Sol Terr Phys* 44–56. <https://doi.org/10.1016/j.jastp.2011.04.024>
- Abdu MA, de Souza JR, Kherani EA, Batista IS, MacDougall JW, Sobral JHA (2015) Wave structure and polarization electric field development in the bottomside F layer leading to postsunset equatorial spread F. *J Geophys Res Space Physics* 120:6930–6940. <https://doi.org/10.1002/2015JA021235>
- Bailey GJ, Balan N, Su YZ (1997) The Sheffield University ionosphere-plasmasphere model—a review. *J Atmos Sol Terr Phys* 59(13):1541–1552
- Bernhardt PA, Ballenthin JO, Baumgardner JL et al (2012) Ground and space-based measurement of rocket engine burns in the ionosphere. *IEEE Trans Plasma Sci* 40:1267
- Bernhardt PT, Huba JD, Kudeki E, Woodman RF, Condori L, Villanueva F (2001) Lifetime of a depression in the plasma density over Jicamarca produced by space shuttle exhaust in the ionosphere. *Radio Sci* 36(5):1209–1220
- Bernhardt PT, Huba JD, Swartz WE, Kelly MC (1998) Incoherent scatter from space shuttle and rocket engine plumps in the ionosphere. *J Geophys Res* V103(A2):2239–2251
- Buonsanto MJ (1994) Evidence for polarization electric fields in the daytime F region above Millstone Hill. *J Geophys Res* 99(A4):6437–6446. <https://doi.org/10.1029/93JA03467>
- Chau JL, Woodman RF (2001) Interferometric and dual beam observations of daytime spread-F-like irregularities over Jicamarca. *Geophys Res Lett* 28(18):3581–3584
- Chen G et al (2017) Low-latitude daytime F region irregularities observed in two geomagnetic quiet days by the Hainan coherent scatter phased array Fucker (HCOPAR). *J Geophys Res Space Physics* 122:2645–2654. <https://doi.org/10.1002/2016JA023628>
- Fejer BG, Jensen JW, Su S-Y (2008) Quiet time equatorial F region vertical plasma drift model derived from ROCSAT-1 observations. *J Geophys Res* 113:A05304. <https://doi.org/10.1029/2007JA012801>
- Fukao S, Ozawa Y, Yamamoto M, Tsunoda RT (2003) Altitude extended equatorial spread F observed near sunrise terminator over Indonesia. *Geophys Res Lett* 30(22):2137. <https://doi.org/10.1029/2003GL018383>
- Huang C-S, de La Beaujardiere O, Roddy PA, Hunton DE, Ballenthin JO, Hairston MR (2013) Long-lasting daytime equatorial plasma bubbles observed by the C/NOFS satellite. *J Geophys Res Space Physics* 118:2398–2408. <https://doi.org/10.1002/jgra.50252>
- Kelley MC (2009) *The Earth's ionosphere: plasma physics and electrodynamics*, 2nd edn. Elsevier, Amsterdam, pp 39–40
- Kelley MC, Ilma RR (2016) Generation of a severe convective ionospheric storm under stable Rayleigh–Taylor conditions: triggering by meteors? *Ann Geophys* 34:165–170
- Li G, Ning B, Abdu MA, Wan W, Hu L (2012) Precursor signatures and evolution of post-sunset equatorial spread-F observed over Sanya. *J Geophys Res* 117:A08321. <https://doi.org/10.1029/2012JA017820>
- Li G, Ning B, Abdu MA, Wan W, Wang C, Yang G, Liu K, Liu L, Yan C (2017) First observation of presunset ionospheric F region bottom-type scattering layer. *J Geophys Res Space Physics* 122. <https://doi.org/10.1002/2016JA023647>
- Li G, Otsuka Y, Ning B, Abdu MA, Yamamoto M, Wan W, Liu L, Abadi P (2016) Enhanced ionospheric plasma bubble generation in more active ITCZ. *Geophys Res Lett* 43:2389–2395. <https://doi.org/10.1002/2016GL068145>
- Li G et al (2010) Longitudinal development of low-latitude ionospheric irregularities during the geomagnetic storms of July 2004. *J Geophys Res* 115:A04304. <https://doi.org/10.1029/2009JA014830>
- Mendillo M, Smith S, Coster A, Erickson P, Baumgardner J, Martinis C (2008) Man-made space weather. *Space Weather* 6:S09001. <https://doi.org/10.1029/2008SW000406>
- Nakashima Y, Heki K (2014) Ionospheric hole made by the 2012 North Korean rocket observed with a dense GNSS array in Japan. *Radio Sci* 49. <https://doi.org/10.1002/2014RS005413>
- Ning B, Hu L, Li G, Liu L, Wan W (2012) The first time observations of low-latitude ionospheric irregularities by VHF radar in Hainan. *Sci China Tech Sci*. <https://doi.org/10.1007/s11431-012-4800-2>

- Otsuka Y, Shiokawa K, Ogawa T, Wilkinson P (2002) Geomagnetic conjugate observations of equatorial airglow depletions. *Geophys Res Lett* 29(15):1753. <https://doi.org/10.1029/2002GL015347>
- Otsuka Y, Shiokawa K, Ogawa T, Yokoyama T, Yamamoto M, Fukao S (2004) Spatial relationship of equatorial plasma bubbles and field-aligned irregularities observed with an all-sky airglow imager and the Equatorial Atmosphere Radar. *Geophys Res Lett* 31:L20802. <https://doi.org/10.1029/2004GL020869>
- Patra AK, Chaitanya PP, Mizutani N, Otsuka Y, Yokoyama T, Yamamoto M (2012) A comparative study of equatorial daytime vertical $E \times B$ drift in the Indian and Indonesian sectors based on 150 km echoes. *J Geophys Res* 117:A11312. <https://doi.org/10.1029/2012JA018053>
- Patra AK, Phanikumar DV (2009) Intriguing aspects of F region plasma irregularities revealed by the Gadanki radar observations during the SAFAR campaign. *Ann Geophys* 27:3781–3790. <https://doi.org/10.5194/angeo-27-3781-2009>
- Pi X, Mannucci AJ, Lindqwister UJ, Ho CM (1997) Monitoring of global ionospheric irregularities using the worldwide GPS network. *Geophys Res Lett* 24(18):2283–2286
- Shume EB, Rodrigues FS, de Paula ER, Batista IS, Butala MD, Galvan DA (2013) Day-time F region echoes observed by the Sao Luis radar. *J Atmos Solar Terr Phys* 103:48–55
- Wang C (2010) New chains of space weather monitoring stations in China. *Space Weather* 8:S08001. <https://doi.org/10.1029/2010SW000603>
- Woodman RF, Pingree JE, Swartz WE (1985) Spread-F-like irregularities observed by the Jicamarca radar during the day-time. *J Atmos Terr Phys* 47(8-10): 867–874. [https://doi.org/10.1016/0021-9169\(85\)90061-3](https://doi.org/10.1016/0021-9169(85)90061-3)
- Yokoyama T, Yamamoto M, Otsuka Y, Nishioka M, Tsugawa T, Watanabe S, Pfaff RF (2011) On post-midnight low-latitude ionospheric irregularities during solar minimum: 1. Equatorial Atmosphere Radar and GPS-TEC observations in Indonesia. *J Geophys Res* 116:A11325. <https://doi.org/10.1029/2011JA016797>
- Zalesak ST, Ossakow SL, Chaturvedi PK (1982) Nonlinear equatorial spread F: the effect of neutral winds and background Pedersen conductivity. *J Geophys Res* 87:151–166

Submit your manuscript to a SpringerOpen[®] journal and benefit from:

- Convenient online submission
- Rigorous peer review
- Open access: articles freely available online
- High visibility within the field
- Retaining the copyright to your article

Submit your next manuscript at ► springeropen.com
